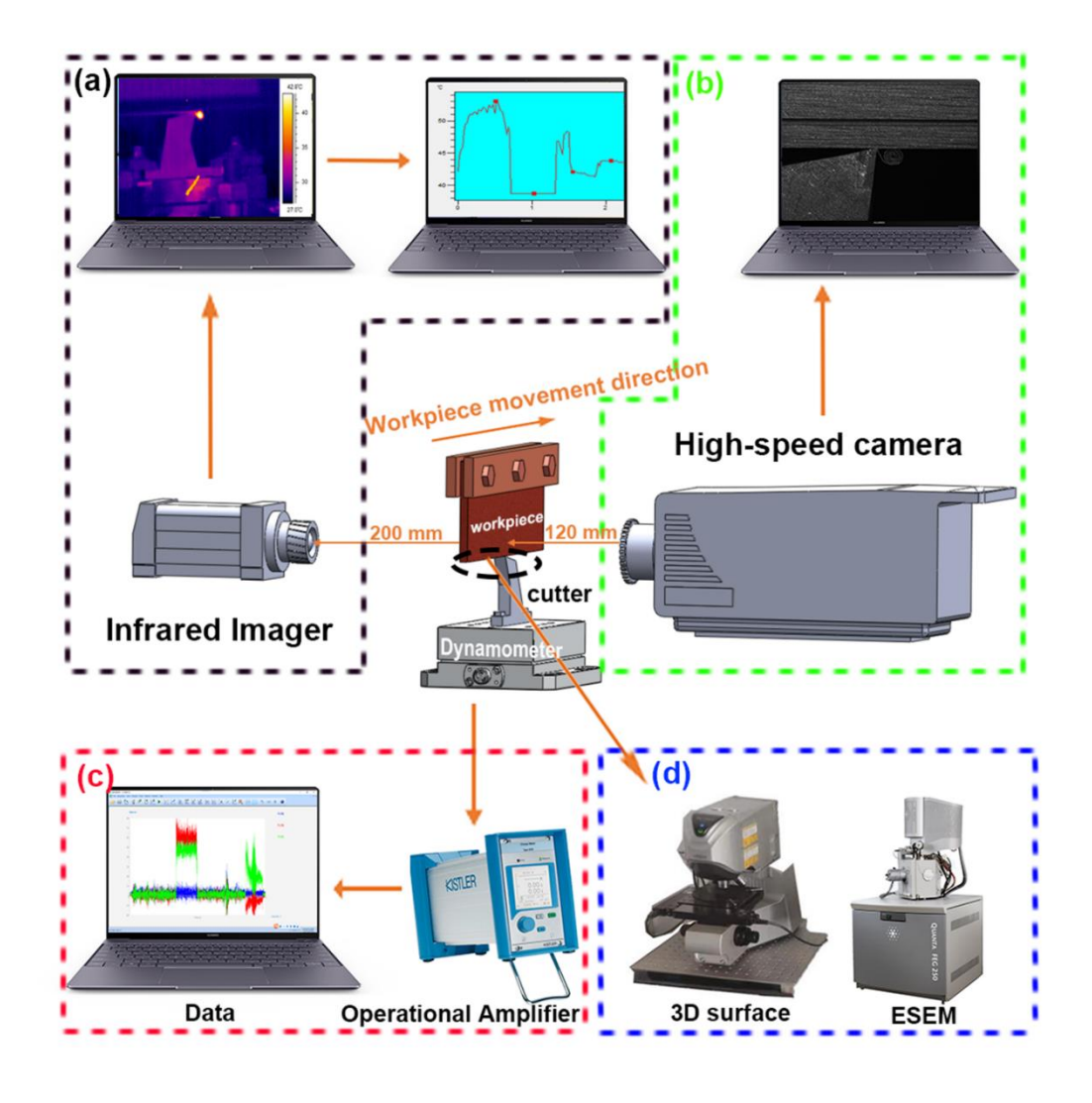
Surface Damage Mechanism and Chip Curling Analysis of Orthogonal Cutting Wood-Plastic Composites

Peiqi Yang,^a Feng Zhang,^a Liyun Qian,^a Zhanwen Wu,^a Bin Na,^a Yutang Chen,^a Qingyang Jin,^a and Jinxin Wang ^{b,*}

DOI: 10.15376/biores.20.3.5246-5261

GRAPHICAL ABSTRACT



^{*} Corresponding author: jackiewang@njfu.edu.cn

Surface Damage Mechanism and Chip Curling Analysis of Orthogonal Cutting Wood-Plastic Composites

Peiqi Yang,^a Feng Zhang,^a Liyun Qian,^a Zhanwen Wu,^a Bin Na,^a Yutang Chen,^a Qingyang Jin,^a and Jinxin Wang ^{b, *}

The machining processing of wood-plastic composites (WPCs) has some technological gaps in the field of surface damage mechanism and surface quality monitoring. In this study, orthogonal cutting tests were used to investigate the mechanisms of surface damage and the degree of chip (the material cutting off by cutting tool) curling of WPCs with various tool rake angles (from 5 ° to 40 °) and cutting depths (from 0.1 to 1 mm). Based on observations of the processed surface micromorphology, a surface damage model is proposed to describe the temperature-dependent reduction in adhesion force between polyethylene and wood flour. Chip curling was quantified by the point curvature in the side view. The curvature data for each chip point were negatively correlated with the depth of cut, but the relationship with the tool rake angle was less pronounced. The surface damage mechanism of WPCs during machining was revealed, providing a theoretical basis for improving surface quality through material formulation. The analysis of chip curvature offers theoretical support for the dynamic observation of chip morphology and elucidates the relationship between chip morphology, cutting depth, and tool rake angle. These findings can serve as a foundation for monitoring cutting precision in practical production.

DOI: 10.15376/biores.20.3.5246-5261

Keywords: WPCs; Orthogonal cutting; Chip curling; Surface damage mechanism; Microscopic damage

Contact information: a: College of Materials Science and Engineering, Nanjing Forestry University, P. O. Box 210037, Nanjing, People's Republic of China; b: College of Furnishings and Industrial Design, Nanjing Forestry University, P. O. Box 210037, Nanjing, People's Republic of China; *Corresponding author: jackiewang@njfu.edu.cn

INTRODUCTION

Wood-plastic composites (WPCs) have emerged as a sustainable alternative in engineering applications due to their cost-effectiveness, dimensional stability, and resistance to degradation (Yáñez-Pacios *et al.* 2017). Their environmental credentials are further strengthened by utilizing recycled thermoplastics and wood residues, aligning with circular economy principles (Li *et al.* 2021; Elsheikh *et al.* 2022).

Manufacturing WPCs involves primary forming processes (*e.g.*, extrusion, injection molding) followed by secondary machining operations, such as drilling and trimming (Gardner *et al.* 2015). However, the presence of the polymer matrix in WPCs introduces machining challenges, notably surface integrity degradation and accelerated tool wear, which constrain industrial adoption.

WPCs are categorized by polymer matrices into three dominant types: polyethylene WPCs (most prevalent in outdoor applications), polypropylene WPCs, and polyvinyl chloride WPCs. The machining performance of polyethylene-based WPCs (most prevalent

in outdoor applications) warrants particular attention, as optimizing their cutting behavior directly enhances production efficiency and cost-effectiveness.

Due to the synergistic effects of various components in WPCs and the microscopic structural differences between wood and thermoplastic plastics, the cutting properties of WPCs are distinct from those of wood or plastic (Li *et al.* 2004). This distinction makes it essential to investigate how cutting parameters affect outcomes such as cutting force, temperature, surface quality, and chip morphology. Previous studies have used statistical methods to analyze these indicators during the cutting process, providing useful insights about cutting parameter (Saloni *et al.* 2011; Guo *et al.* 2014a, b; Nairn 2016; Zhu *et al.* 2017; De Luycker 2022). However, this study is focused on chip curling, which addresses gaps in existing research and offers new perspectives on how these parameters influence the machining performance of WPCs.

The study of chip formation is also crucial in secondary machining processes. During the machining process of wood-plastic composites, the differences in chip curvature may stem from their unique structural and compositional characteristics. Compared to wood, the presence of a polymer matrix in WPCs alters the material's mechanical behavior and fracture modes (Li et al. 2004). In contrast to pure polymers, the addition of wood fibers significantly enhances the material's rigidity. The combined effects of these factors may lead to the formation of distinct chip morphologies and curvatures during the machining of WPCs. Historical research has investigated key factors such as shear strain, shear rate, and chip flow rate in metal cutting (Merchant 1945). The morphology of cutting chips, including side and internal views, has been analyzed using scanning electron microscopy to compare differences between metal and bone chips, leading to the proposal of a new cutting model that accounts for the viscoelasticity of bone (Wang et al. 2023). The effect of fiber orientation and cutting depth on chip shape and size during carbon fibre-reinforced polymer cutting has been studied, with various approaches using scanning electron microscopy to observe and classify chip morphology (De Luycker et al. 2022; Usca et al. 2022; Zheng et al. 2023). Additionally, finite element analysis has been employed to investigate the impact of cutting conditions on chip formation and surface damage in porous metals (Guerra Silva et al. 2021). These papers demonstrated the feasibility of utilizing chip characteristics as key indicators to study the surface damage mechanisms of WPCs, helping this study to develop a cutting model applicable to WPCs.

In this work, based on the observation of the micromorphology of processed surfaces, a surface damage model is proposed that accounts for the temperature-dependent decrease in adhesion between polyethylene and wood flour. In addition, a new method to quantify chip curling is proposed: the point curvature of different chips was measured using ImageJ. The aim of this thesis was to elucidate the surface damage mechanism and the variation of chip morphology of WPCs during machining, and to provide the principle support for process monitoring of cutting accuracy in industrial production scenarios.

EXPERIMENTAL

Materials

The polyethylene WPCs used in this study were supplied by Huangshan Mason Plastic Wood New Material Technology Co., Ltd. (Huangshan, China) and consisted mainly of mixed wood powder and polyethylene with a mass fraction of 60% wood powder and 30% polyethylene, and the rest consisted of additives such as lubricants, maleic

anhydride grafted polyethylene (MAPE, to reduce air gaps), and pigments, namely carbon nanotubes. The average particle size of wood powder in polyethylene WPCs was 0.25 mm (60 mesh). The polyethylene was obtained by recycling. Such material has a relatively low melting temperature, usually between 106 and 130 °C. It was mixed thoroughly with the mixed wood powder and extruded at 150 °C. The physical and mechanical properties of the WPCs workpieces were tested using a universal mechanical testing machine, and the data, Table 1.

 Table 1. Mechanical Properties of Polyethylene WPCs

Wood Flour Mass Fraction (%)	Polyethylene Mass fraction (%)	Flexural Strength (MPa)	Modulus of Elasticity (MPa)	Density (g/cm³)
60	30	4.69	4.27	1.12

The tools used in this test were produced by Leitz Co., Ltd. (Nanjing, China). The tool base is carbon tool steel, and the insert is inlaid with cemented YG8 carbide. The advantages of the tool are high toughness of the tool body and high hardness of the tool head, whose tensile strength (MPa), flexural strength (MPa) and hardness (HRC) are 890, 1470 and 75, respectively. The angular parameters and dimensions of the tool, Table 2.

Table 2. Tools Angle Parameters

No.	Rake angle (°)	Wedge angle (°)	Clearance angle (°)
1	5	78	12
2	15	73	12
3	25	63	12
4	30	58	12
5	40	48	12

Methods

Cutting tests were performed on a planer (B665, Shenyang No. 1 Heavy Machine Tool Factory, Shenyang, China), as shown in Fig. 1. The cutting speed of this machine was set to be constant, i.e., 17.9 m/min, and the cutting depth was from 0.1 to 1.0 mm. Specific cutting depths were 0.1, 0.3, 0.5, 0.7, and 1.0 mm, respectively. The force measuring instrument was fixed on the planer table by a fixture. The tool was fixed to the upper surface of the force gauge by the fixture. Its cutting edge was parallel to the X-axis direction of the force measuring instrument, and the side surface of the tool was perpendicular to the cutting edge and parallel to the Y-axis direction of the force measuring instrument. The workpiece was fixed on the tool holder of the planer by the fixture. Its length direction was parallel to the Y-axis direction of the force gauge, and its thickness direction was parallel to the Xaxis direction of the force gauge. From the Y-axis of the force measuring machine, the workpiece and the tool were mounted symmetrically about the Z-axis of the force measuring machine, and the workpiece was fed in the Y-axis by the slide rail. In this work, the orthogonal cutting performance of polyethylene WPCs was investigated by varying the cutting depth and tool rake angle among the experimental parameters. The experiment was conducted as a full factorial design (Table 3). Each dataset presented in the table is the average of four parallel experiments, where γ represents the tool rake angle, h represents cutting depth, F represents the cutting force, T represents the cutting temperature, and STDEV represents the standard deviation of the samples, which reflects the degree of discretization of each value with respect to the mean value. The cutting temperature was collected using an infrared imager (Thermo Vision A20-M, FLIR Systems Inc., USA) at a frequency of 50 Hz. The highest temperature at the contact position between the cutting edge and the workpiece was selected as the experimental data in postprocessing, as illustrated in Fig. 1a. To observe the chip formation process in the experiment, a high-speed camera (I-speed 3, Olympus Co., Ltd., Tokyo, Japan) was used to acquire cutting images at 5000 frames per second, as shown in Fig. 1b.

At the same time, a force measuring instrument (Kistler 9257B, Kistler Group, Winterthur, Switzerland) was used to obtain cutting forces in three directions (F_x , F_y , F_z), *i.e.*, lateral, parallel, and normal forces. The setup and data acquisition are depicted in Fig. 1c. The cutting forces were sampled by the force measuring instrument at a frequency of 7142 Hz and transmitted to the signal operation amplifier to obtain the cutting force data. Each dataset is the average of five experiments. The cutting force is a composite of F_y and F_z , and the cutting force can be obtained by Eq. 1.

$$F = \sqrt{F_V^2 + F_Z^2} \tag{1}$$

After the cutting test, the 3D profile of the machined workpiece surface was measured by the Keyence 3D surface profiler, as shown in Fig. 1d on the left, which shows the bumps and pits on the machined surface. This method allows further analysis of the surface quality by the VK analysis software. To gain deeper insights into the surface profile characteristics, the 3D profile of the machined surface was also examined using an environmental scanning electron microscope, as shown in Fig. 1d on the right.

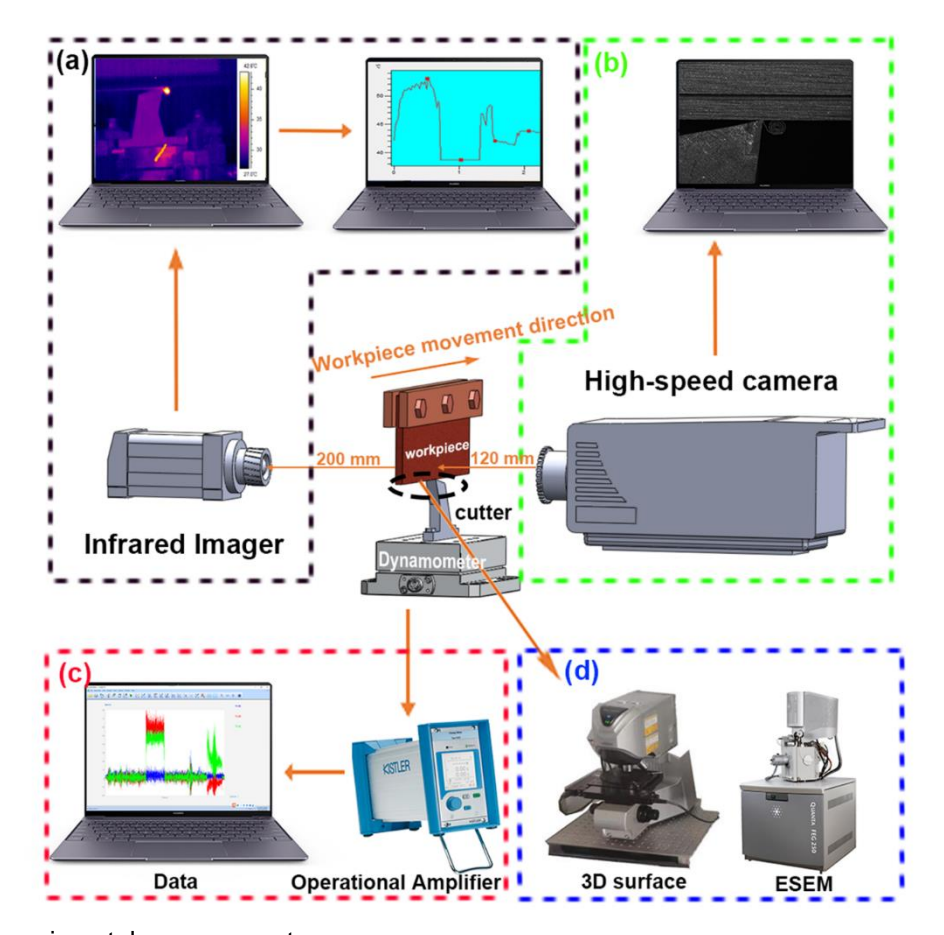


Fig. 1. Experimental arrangement

RESULTS AND DISCUSSION

Effect of Cutting Parameters on Cutting Force and Cutting Temperature

The cutting force F calculated by Eq. 1 (for mechanical analysis) and the cutting temperature T measured by infrared imager respectively show their variation trends with rake angle γ and cutting depth h in Fig. 2. The variation law of the cutting force and cutting temperature was not dramatically different from that in previous studies (Saloni $et\ al.\ 2011$; Guo $et\ al.\ 2014$; Guo $et\ al.\ 2014$; Zhu $et\ al.\ 2017$). The analysis of the variation law is mainly based on the sources of the cutting force, the three major deformation zones and the cutting temperature (Zhang $et\ al.\ 2021$).

First, it was discovered that both cutting force and cutting temperature tended to rise as the cutting depth rose. This can be appreciated by looking at the figure from the left vertical coordinate in the image. The thickness of the chip that the tool separates off is known as the cutting depth, and as the chip thickness rose, so did the pressure and shear forces acting on the initial deformation zone, thereby increasing the cutting force. Because of the increased cutting force in this area, there was also more friction between the front tool surface and the chip, which produced frictional heat and serves as the main source of cutting heat, explaining why the trend of temperature change was almost identical to the trend of cutting force change. The image also shows a minor trend for the cutting force and temperature to decrease as the rake angle of the tool increases. The cutting force was

reduced due to the increased concentration of the tool's compressive stress on the workpiece and the ease with which the chips could be separated as the wedge angle decreased. The wedge angle lowered the friction between the tool's front surface and the chip, which lowered the cutting temperature.

Finally, the figure contains a unique piece of information: in Fig. 2, where $\gamma=5$ ° and h=0.1 mm, the cutting force was very small, but the cutting temperature was very high. Due to the tool rake angle and cutting depth being too small, the second deformation zone was hard to produce, and the front tool surface pressing against the material made the friction so fierce that a large amount of heat was produced. What's more, due to the cutting depth being so small, that allowed the material to be removed with smaller cutting forces.

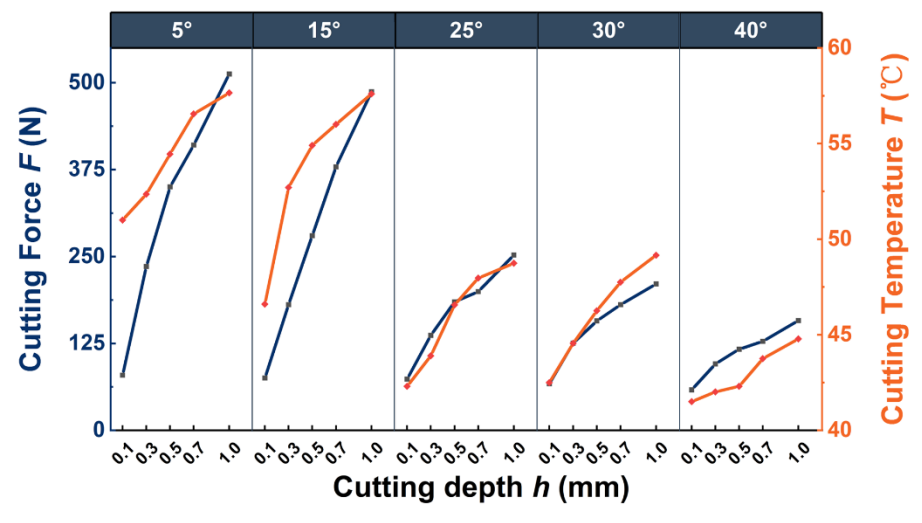


Fig. 2. Influence of cutting parameters on cutting force and cutting temperature. Different tool rake angles are shown in the upper horizontal axis.

Effect of Cutting Parameters on Surface Topography

Photos of chip formation and 3D surface morphology for different cutting depths of the same rake angle are illustrated in Fig. 3. It could be seen by the naked eye and the side view of the machined surface. The 3D morphological parameters of the machined surface were measured using VK analysis software. It was discovered that when the cutting depth increased, the chip curl decreased, and excessive extrusion-related chip breaking increased. The machined surface simultaneously becomes more uneven, primarily in the form of pits and burrs.

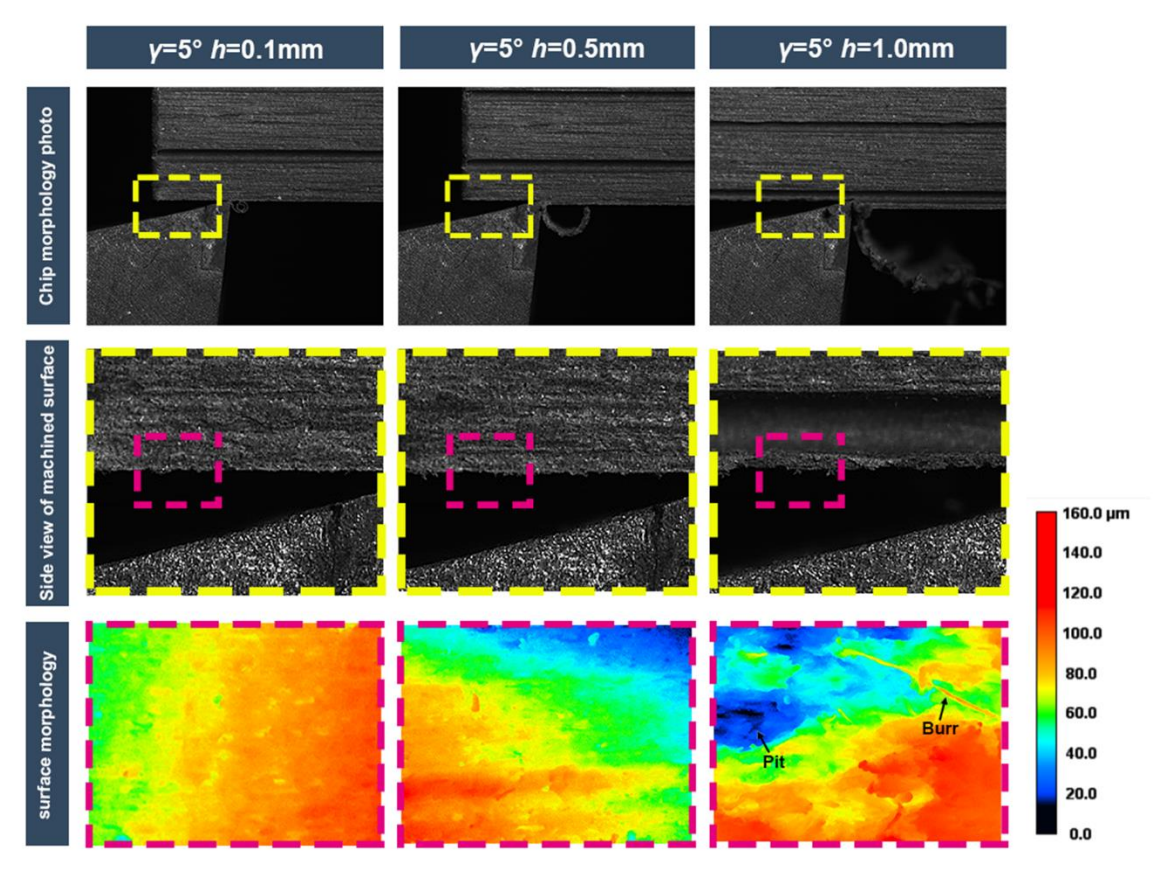


Fig. 3. Comparison photo of the same rake angle (γ =5°) with different cutting depths (h=0.1 mm; h=0.5 mm; h=1.0 mm)

The chip morphology and the side view of the machined surface are both clearly visible, as illustrated in Fig. 4. The 3D morphological properties of the machined surface were analyzed using VK analysis software. It was discovered that the chip curl steadily rose as the tool rake angle increased, especially between 5 $^{\circ}$ and 25 $^{\circ}$, but beyond 25 $^{\circ}$, the chip curling did not vary considerably.

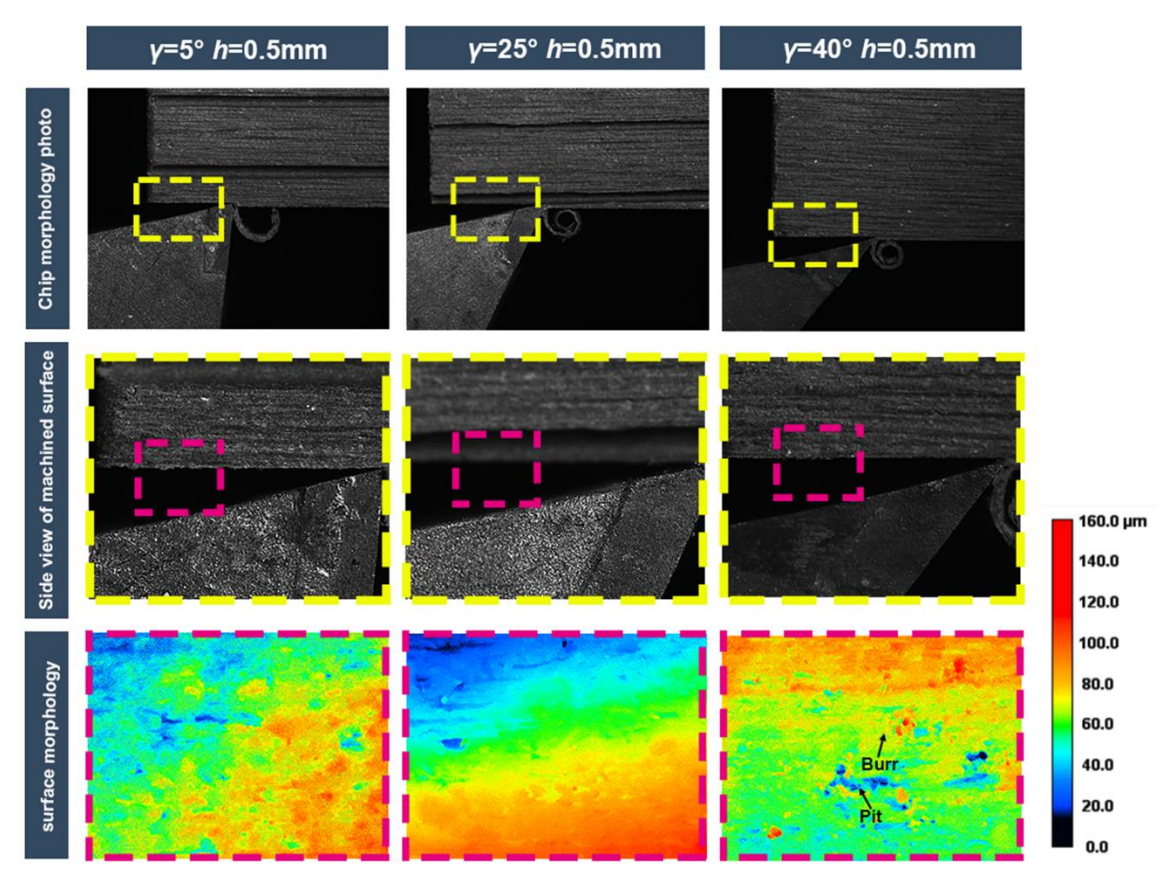


Fig. 4. Comparison photo of the same cutting depth (h=0.5 mm) with different rake angles (γ =5 °; γ =25 °; γ =40 °)

Machined Surface Analysis

The surface flaws are pits and their accompanying bumps, as shown by the comparison of various image sets (Figs. 5 and 6). These faults were constantly smaller than 0.25 mm in length in one direction, which is in line with the particle size of the wood powder, as shown by the existence of pits that pass through the 60 mesh sieve. This assessment is supported by the fact that the elastic modulus of wood fibers is approximately 40 times higher than that of polyethylene and the strength is approximately 20 times higher and good dispersion and strong interfacial adhesion between the hydrophilic wood and the hydrophobic polymers are difficult to achieve as well as the fact that polyethylene softens at high temperatures.

It is thought that the cutting damage of polyethylene WPCs is caused by insufficient wood powder to polyethylene adhesion under the influence of temperature (Bengtsson *et al.* 2005; Niska *et al.* 2008). According to the scanning electron microscopy images, it can be observed that the damage was not entirely caused by the detachment of single fibers, indicating that even sieved fibers may exhibit agglomeration. For different WPCs, the size of the damage may be related to whether the interfacial detachment involves a single fiber or multiple fibers. In studies on the machining surface damage mechanisms of WPCs with varying wood flour content (Zhu 2023), researchers found that higher wood flour content resulted in greater surface roughness, indirectly confirming the role of wood flour content in surface damage and further substantiating that wood flour disruption is a primary cause of surface damage.

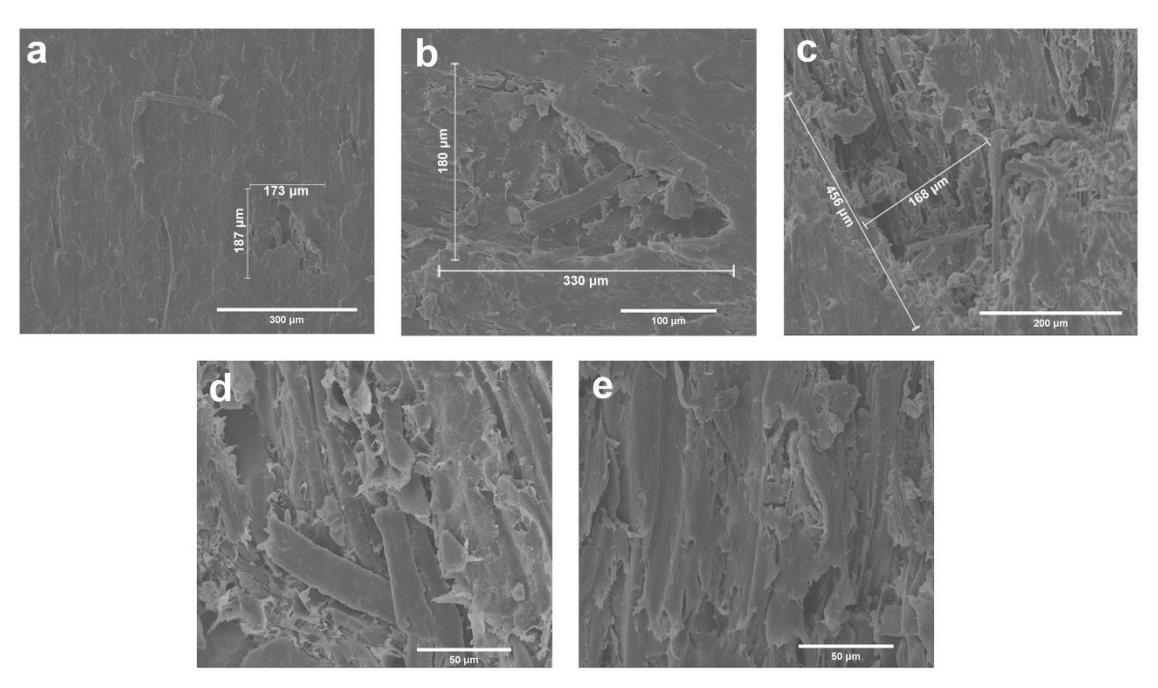


Fig. 5. Environmental scanning electron microscopy (ESEM) image of machined surfaces with different cutting depths (a. h=0.1 mm, b. h=0.3 mm, c. h=0.5 mm, d. h=0.7 mm, e. h=1.0 mm) at the same rake angle (γ =15 °)

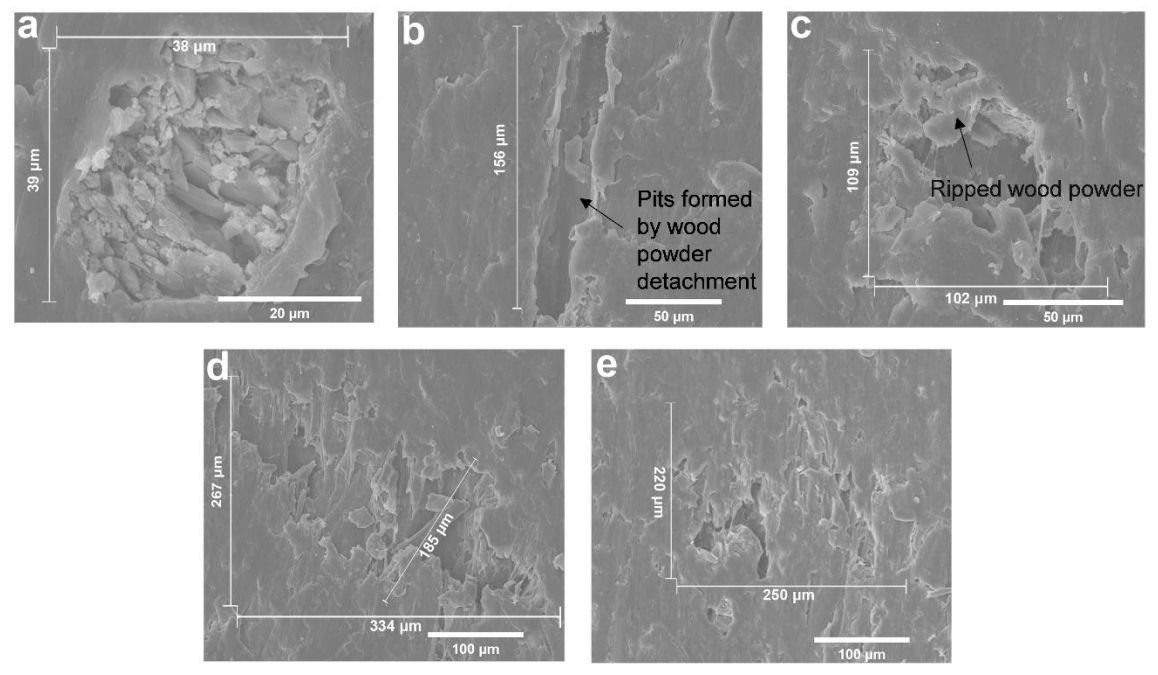


Fig. 6. Environmental scanning electron microscopy image of machined surfaces with different rake angles (a. $\gamma=5$ °, b. $\gamma=15$ °, c. $\gamma=25$ °, d. $\gamma=30$ °, e. $\gamma=40$ °) at the same cutting depth (h=0.5 mm)

The model diagram shows that the cutting damage of polyethylene WPCs was mainly due to the shedding of wood flour particles, as shown in Fig. 7. To make the model more rigorous, a form of damage in which part of the wood flour and part of the polyethylene is torn is also proposed.

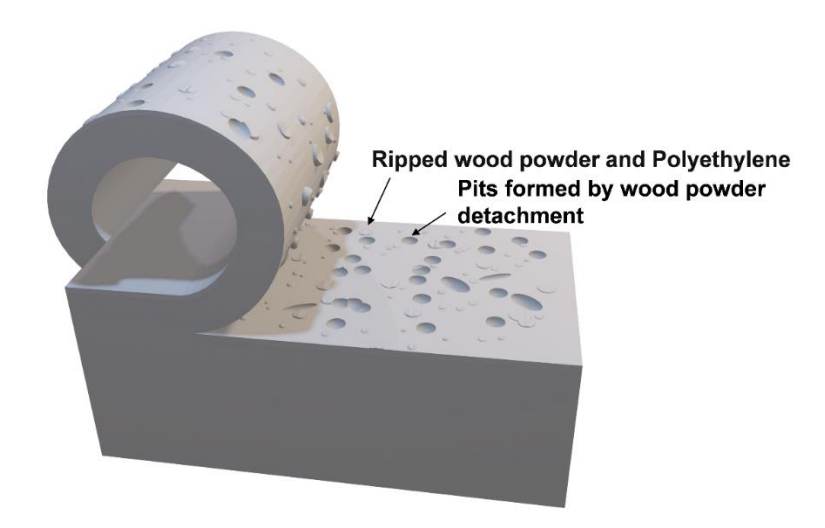


Fig. 7. polyethylene WPCs cutting damage model

Chip Point Curvature Analysis

It is evident that the curl degree of each chip varied with different cutting depths, as shown in Fig. 8. In this study, the point curvature data on each chip were gathered using the kappa plug-in on ImageJ, as shown in Fig. 5 on the left. The point curvature data were then divided into five groups based on different depths of cut, and five sets of chip curvature simulation plots with X coordinates in the horizontal coordinate and Y coordinates in the vertical coordinate were produced, as illustrated in Fig. 5 on the right. The lower left corner of the high-speed camera's photograph serves as the origin for the mockups, which have μm for both their horizontal and vertical coordinates.

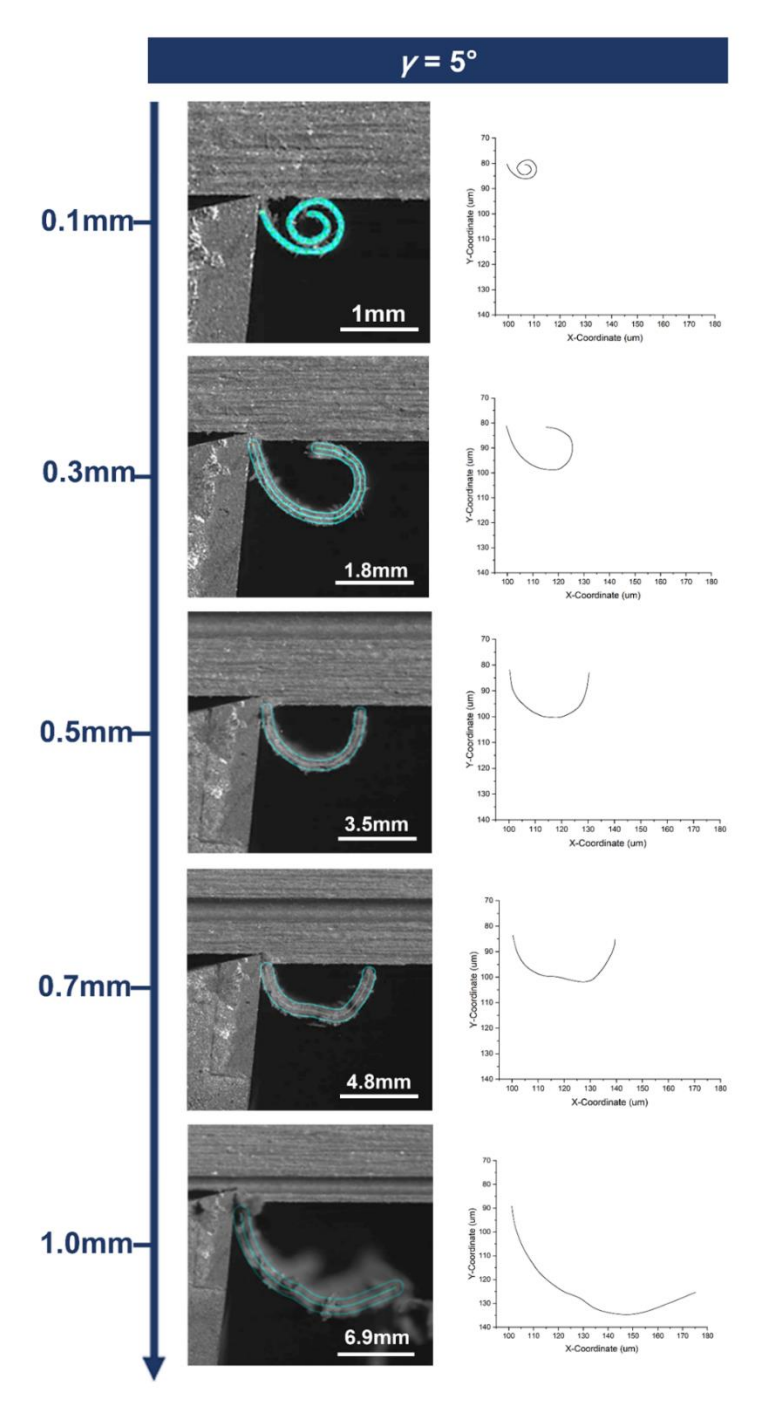


Fig. 8. Chip formation diagram for different cutting depths for the same rake angle (γ =5°)

In Fig. 9, the point curvature is represented by the vertical coordinates, while the five distinct depths of cut are represented by the horizontal coordinates. The horizontal line inside the box denotes the median value of the dataset, the dot denotes the mean value of the collection of data, and the two horizontal lines jutting out from the box denote the maximum and minimum values of the data. The box's upper and bottom borders correspond to the data's upper and lower quartiles, respectively. The decreased cutting depth causes the cutting force to be concentrated on a smaller cutting area, increasing its

impact on the degree of chip bending. As a result, the amount of chip bending diminishes as the cutting depth increases because the cutting force is spread more uniformly and the cutting pressure drops. Second, the chip length dramatically increases as the cutting depth decreases, and a longer chip length facilitates free turning and twisting, suggesting that it is simpler to maintain a higher degree of bending (Nairn 2016).

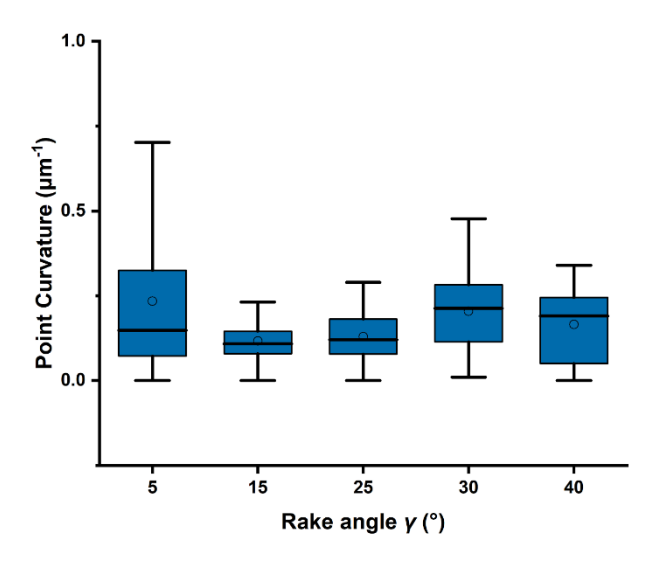


Fig. 9. Comparison of point curvature at different cutting depths

At the same cutting depth (h=0.5 mm), it is evident that the curvature degree of each chip varies for various tool rake angles, as illustrated in Fig. 10. The Kappa plug-in of ImageJ was used to collect the curvature data of each point on each chip in this study, as illustrated in Fig. 10 on the left. The data were then divided into five groups based on various tool rake angles, and five sets of chip curl degree simulation graphs with X coordinates in the horizontal coordinate and Y coordinates in the vertical coordinate were created, as illustrated in Fig. 10 on the right. To compare the point curvature under various tool rake angles, the five sets of point curvature data were converted into box line plots. It was observed that an increase in the tool rake angle had minimal impact on the point curvature of the chips, as illustrated in Fig. 11. This is because altering the tool's rake angle may result in a slight alteration in the size and direction of the cutting force acting on the chip, which obscures any change in the chip's curvature at any given spot. It is important to take into account all of the factors that affect chip behavior, including the interaction between tool rake angle and other cutting circumstances.

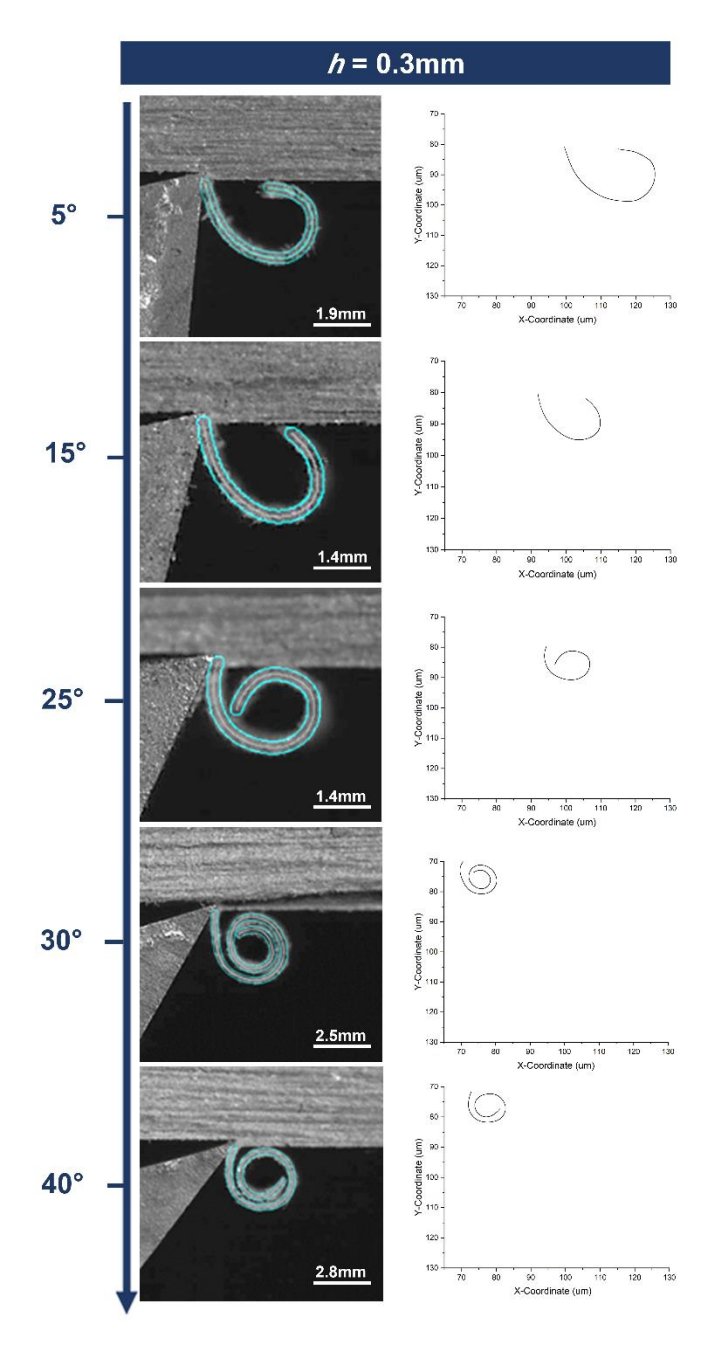


Fig. 10. Chip formation diagram for different rake angles for the same depths of cut (*h*=0.3)

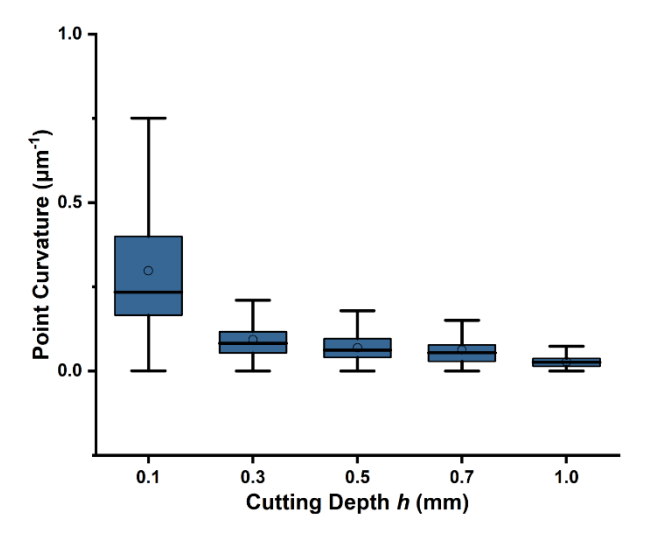


Fig. 11. Comparison of point curvature at different rake angles

CONCLUSIONS

- 1. Cutting parameters, which vary in cutting force and temperature, have an impact on chip formation. In the case of recycled polyethylene that was reinforced with wood power and with maleic anhydride grafted polyethylene (MAPE), the cutting depth was positively correlated with both the cutting force and cutting temperature, and the rake angle was negatively correlated with both the cutting force and cutting temperature.
- 2. The surface irregularity of the machined surface increased and the degree of chip curl decreased as the cutting depth rose. The temperature during the cutting process can weaken the connection between polyethylene and wood powder in polyethylene WPCs, which results in surface degradation. ESEM images revealed that the damage resulted from both single and agglomerated fiber detachment, which was likely due to fiber agglomeration post-sieving. Consequently, damage size in WPCs may depend on single or multiple fiber detachment, highlighting the need to study cutting parameters and properties under supercritical CO₂ conditions.
- 3. The degree of curvature of each chip showed the effect of chip extrusion and deformation on the front tool surface, and a new method for collecting data on the degree of chip bending was proposed. The curvature data for each chip point were negatively correlated with the depth of cut, but the relationship with the tool rake angle was less pronounced.

ACKNOWLEDGMENTS

The authors are grateful for the support of the National Natural Science Foundation of China (NSFC) [32471791] and the Postgraduate Research Practice Innovation Program of Jiangsu Province [SJCX22_0317].

REFERENCES CITED

- Bengtsson, M., Gatenholm, P., and Oksman, K. (2005). "The effect of crosslinking on the properties of polyethylene/wood flour composites," *Compos Sci Technol* 65(10), 1468-1479. DOI: 10.1016/j.compscitech.2004.12.050
- Elsheikh, A. H., Panchal, H., Shanmugan, S., Muthuramalingam, T., El-Kassas, A. M., and Ramesh, B. (2022). "Recent progresses in wood-plastic composites: Preprocessing treatments, manufacturing techniques, recyclability and eco-friendly assessment," *Cleaner Engineering and Technology* 8, article 100450. DOI: 10.1016/j.clet.2022.100450
- Gardner, D. J., Han, Y., and Wang, L. (2015). "Wood–plastic composite technology," *Current Forestry Reports* 1(3), 139-150. DOI: 10.1007/s40725-015-0016-6
- Guerra Silva, R., Teicher, U., Ihlenfeldt, S., and González-Zamora, A. (2021). "Finite element analysis of orthogonal cutting of cellular metals: influence of cutting conditions on chip formation and surface damage," *The International Journal of Advanced Manufacturing Technology* 113, 1267-1280. DOI: 10.1007/s00170-021-06689-0
- Guo, X., Ekevad, M., Grönlund, A., Marklund, B., and Cao, P. (2014a). "Tool wear and machined surface roughness during wood flour/polyethylene composite peripheral up-milling using cemented tungsten carbide tools," *BioResources* 9(3), 3779-3791. DOI: 10.15376/biores.9.3.3779-3791
- Guo, X., Ekevad, M., Marklund, B., Li, R., Cao, P., and Grönlund, A. (2014b). "Cutting forces and chip morphology during wood-plastic composites orthogonal cutting," *BioResources* 9(2), 2090-2106. DOI: 10.15376/biores.9.2.2090-2106
- Li, D. G., Min, Z., and Li-Jun, F. (2004). "Comparative the main mechanical properties of WPC and wood," *Packaging Engineering* 03, 152-153+222.
- Li, Y., and Wang, B. (2021). "Go green and recycle: Analyzing the usage of plastic bags for shopping in China," *International Journal of Environmental Research and Public Health* 18(23), article 12537. DOI: 10.3390/ijerph182312537
- Luycker, E., Lachaud, F., and Miah, F. (2022). "Minimum cutting depth and cutting depths' effects to chip's shape and size in orthogonal cutting of CFRP," *International Journal of Machining and Machinability of Materials* 23(5/6), 1-1. DOI: 10.1504/IJMMM.2022.10042948
- Merchant, M. (1945). "Mechanics of the metal cutting process. I. Orthogonal cutting and a Type 2 chip," *Journal of Applied Physics* 16, 267-275. DOI: 10.1063/1.1707586
- Mital, D., Hatala, M., Zajac, J., Michalik, P., Duplak, J., Vybostek, J., Mroskova, L., and Knežo, D. (2017). "Study of cutting zone of WPC material after cold cutting," in: *SmartCity360 2016 Conference*, Bratislava, Slovakia.
- Nairn, J. A. (2016). "Numerical modelling of orthogonal cutting: Application to woodworking with a bench plane," *Interface Focus* 6, 20150110-20150110. DOI: 10.1098/rsfs.2015.0110
- Niska, K., and Sanadi, A. (2008). "3 Interactions between wood and synthetic polymers," in: *Wood Polymer Composites*, Kristiina Oksman Niska, Mohini Sain. (ed.), Springer, Singapore. DOI: 10.1533/9781845694579.41.
- Saloni, D., Buehlmann, U., and Lemaster, R. (2011). "U tool wear when cutting wood fiber–plastic composite materials," *Forest Products Journal* 61, 149-154. DOI: 10.13073/0015-7473-61.2.149
- Shi, W., Ma, Y., Yang, C., Jiang, B., and Li, Z. (2017). "Evaluation of a regression

- prediction model for surface roughness of wood-polyethylene composite (WPC)," *Surface Review and Letters* 24, 1850033-1850033. DOI: 10.1142/S0218625X18500336
- Usca, Ü., Uzun, M., Şap, S., Kuntoğlu, M., Giasin, K., Pimenov, D., and Wojciechowski, S. (2022). "Tool wear, surface roughness, cutting temperature and chips morphology evaluation of Al/TiN coated carbide cutting tools in milling of Cu-B-CrC based ceramic matrix composites," *Journal of Materials Research and Technology* 16, 1243-1259. DOI: 10.1016/j.jmrt.2021.12.063
- Wang, H., Satake, U., and Enomoto, T. (2023). "Serrated chip formation mechanism in orthogonal cutting of cortical bone at small depths of cut," *Journal of Materials Processing Technology* 319, 118097-118097. DOI: 10.1016/j.jmatprotec.2023.118097
- Yáñez-Pacios, A. J., and Martín-Martínez, J. M. (2017). "Surface modification and improved adhesion of wood-plastic composites (WPCs) made with different polymers by treatment with atmospheric pressure rotating plasma jet," *International Journal of Adhesion and Adhesives* 77, 204-213. DOI: 10.1016/j.ijadhadh.2017.06.001
- Zhang, F., Wu, Z., Hu, Y., Zhu, Z., and Guo, X. (2021). "Prediction of cutting temperature in the milling of wood-plastic composite using artificial neural network," *BioResources* 16(4), 6993-7005. DOI: 10.15376/biores.16.4.6993-7005
- Zheng, Z., Guo, J., Gao, R., and Jin, X. (2023). "Research on the cutting force and serrated chips in ultra-precision micro-grooving of SLM Ti6Al4V alloy," *Micromachines* 14, 533-533. DOI: 10.3390/mi14030533
- Zhu, M. (2023). Study on Material Deformation Mechanism in Cutting Area of Woodplastic Composites, Master's Thesis, Nanjing Forestry University, Nanjing, China. DOI: 10.27242/d.cnki.gnjlu.2023.000226.
- Zhu, Z., Guo, X., Ekevad, M., Cao, P., Na, B., and Zhu, N. (2017). "The effects of cutting parameters and tool geometry on cutting forces and tool wear in milling high-density fiberboard with ceramic cutting tools," *The International Journal of Advanced Manufacturing Technology* 91(9), 4033-4041. DOI: 10.1007/s00170-017-0085-8

Article submitted: January 10, 2025; Peer review completed: March 15, 2025; Revised version received: April 11, 2025; Accepted: April 12, 2025; Published: May 6, 2025. DOI: 10.15376/biores.20.3.5246-5261